Journal of Catalysis 391 (2020) 404–413

Contents lists available at ScienceDirect

Journal of Catalysis

journal homepage: www.elsevier.com/locate/jcat

The effect of Si environments on NH_3 selective catalytic reduction performance and moisture stability of Cu-SAPO-34 catalysts

Yi Cao [a,b], Dong Fan [b], Dali Zhu [b,c], Lijing Sun [b,c], Lei Cao [b], Peng Tian [b,*], Zhongmin Liu [b,*]

[a] School of Material Science and Chemical Engineering, Ningbo University, Ningbo 315211, People's Republic of China
[b] National Engineering Laboratory for Methanol to Olefins, Dalian National Laboratory for Clean Energy, Dalian Institute of Chemical Physics, Chinese Academy of Sciences, Dalian 116023, People's Republic of China
[c] University of Chinese Academy of Sciences, Beijing 100049, People's Republic of China

ARTICLE INFO

Article history:
Received 21 February 2020
Revised 1 September 2020
Accepted 1 September 2020
Available online 11 September 2020

Keywords:
Cu-SAPO-34
Si environments
NH_3 selective catalytic reduction
Moisture stability
Si content

ABSTRACT

SAPO-34s with varying Si content templated by bulky tetraethylammonium hydroxide (TEAOH) were prepared to investigate the effect of Si environments on the selective catalytic reduction (SCR) of NO_x and the moisture stability of Cu-SAPO-34 catalysts. These Cu-SAPO-34s have similar Cu loadings, isolated Cu^{2+} content, and Brønsted acid sites (BAS). Both the ratio of Si islands and the acid strength of Cu-SAPO-34s increase with increasing Si content. In situ diffused reflection infrared Fourier transform spectroscopy (DRIFTS) studies reveal that the NH_3 adsorbed on mild BAS (associated with Si(4Al) species) is more active for NO_x conversion than NH_3 adsorbed on strong ones (associated with Si islands). This agrees well with the high turnover frequency (TOF) and the low activation energy on Cu-SAPO-34 with low Si content and abundant Si(4Al) species (sample Si-7.7). Upon hydration treatment, the textural properties, strong acid sites, and reducibility of isolated Cu^{2+} ions show a decrease. This deterioration intensifies with the increasing Si islands in the catalysts due to the easier occurrence of Si migration and the formation of larger Si islands. Sample Si-7.7 exhibits the best moisture stability and thus well-preserved denitration performance. These results imply that a practical Cu-SAPO-34 catalyst with superior activity and moisture stability may be achieved by controlling the Si environments of SAPO-34 templated by bulky amines.

1. Introduction

Emission of NO_x from lean-burn engines promotes the formation of haze, which causes harmful effects on human health and the environment [1–3]. To reduce NO_x emissions, NH_3 selective catalytic reduction (SCR) technology has been applied in the after-treatment systems of diesel vehicles [4,5]. A typical after-treatment system is composed of an oxidation unit (DOC), a diesel particle filter unit (DPF), an SCR unit, and an NH_3 slip control unit (ASC). During the periodic regeneration of DPF, the SCR catalyst inevitably encounters high temperatures with vapor [6]; thus, extraordinary hydrothermal stability is needed. It has been recognized that Cu-SAPO-34 is one of the best catalysts with great NH_3 SCR performance, high N_2 selectivity, and excellent high-temperature hydrothermal stability, although its low-temperature hydrothermal stability needs to be improved to meet the requirements of practical application [7,8].

Active sites, carrier properties, and the NH_3-SCR process of Cu-SAPO-34 catalysts have been explored widely. Wang et al. proved that the Cu^{2+} ions on the exchange sites are active sites over Cu-SAPO-34 [9]. Xue et al. utilized EPR and the H_2-TPR technique to further confirm that the active sites are isolated Cu^{2+} ions, which are located under the double-six-rings of SAPO-34 [10]. The effects of the carrier properties and acidity were also investigated. Wang et al. [11] and Petitto and Delahay [12] explored the influence of Si content upon NO_x conversion by Cu-SAPO-34 catalyst. They found that the acid content of Cu-SAPO-34 increased with the Si content, so the NH_3 SCR performance was improved. Yu et al. further found that the amount of Si species and the type of template in the gel can be used to adjust the content of acid sites over SAPO-34, which is correlated to the activity of Cu-SAPO-34 [13,14]. In addition, the role of acid site types in the NH_3-SCR process has been explored [15]. It is indicated that the adsorbed NH_3 on Brønsted acid sites (BAS) could migrate to Lewis acid sites (LAS) to participate in the reaction. Su et al. further demonstrated that the adsorbed NH_3 on both LAS and BAS are active [16]. Moreover, to study the effect of BAS on the NO_x conversion of Cu-SAPO-34, the K^+ ion was used to replace H^+ over Cu-SAPO-34, and the results

* Corresponding author.
E-mail addresses: tianpeng@dicp.ac.cn (P. Tian), liuzm@dicp.ac.cn (Z. Liu).

https://doi.org/10.1016/j.jcat.2020.09.002
0021-9517/

revealed that a decrease of BAS resulted in degradation of activity [17]. Ma et al. also proposed that the NH_3 on BAS was active for NH_3-SCR, based on in situ DRIFTS and TPSR results [18]. These results imply that the NH_3-SCR performance is highly correlated with the BAS over Cu-SAPO-34.

It is well known that the formation of BAS on SAPO molecular sieves can be regarded as the incorporation of Si atoms into a neutral AlPO framework [19]. The acid strength of Si environments has the order Si(1Al) > Si(2Al) > Si(3Al) > Si(4Al) [20], which contributes to the variety of acid strength of BAS over SAPO molecular sieves. So far, although the impact of acid amount upon NO_x conversion on Cu-SAPO-34 has been clarified by many researchers as discussed above, less is known about the relationship between the acid strength (Si environments) and the NH_3-SCR performance, which is important for improving the catalyst activity.

On the other hand, Cu-SAPO-34 is sensitive to low-temperature moisture, which limits its practical application. Leistner and Olsson suggested that the deterioration of Cu-SAPO-34 after low-temperature hydration was caused by the loss of active copper species [21]. Wang et al. considered that the destruction of the skeleton and the decrease of acid sites and active sites led to deactivation of the catalyst, and the existence of Cu^{2+} ions would improve the low-temperature hydration stability through the decrease of naked BAS [22]. Recently, Wang et al. utilized 2-D EPR technology to study hydrated Cu-SAPO-34. They found that transformation of active isolated Cu^{2+} ions into $CuAl_2O_4$ led to the deactivation of Cu-SAPO-34 [23]. Our recent study revealed that the decay of strong acid sites and the decrease of Cu^{2+} reducibility to Cu^{+} upon hydration treatment resulted in activity loss by Cu-SAPO-34 [24]. In addition, Huang et al. demonstrated that Cu-SAPO-34 with smaller crystal size showed higher hydration stability due to the gradient distribution of Si [25]. Niu et al. [26] and Xiang et al. [27] improved the low-temperature hydration stability of Cu-SAPO-34 by doping Ce^{3+} or Ag^{+} ions. We found that there was residual NH_3 on the surfaces of catalysts after the SCR reaction, which can effectively enhance the hydrothermal stability of Cu-SAPO-34 below 300 °C [28].

Additionally, the choice of an organic template for the synthesis of SAPO-34 also affects the moisture stability of SAPO-34/Cu-SAPO-34. Woo et al. found that the NH_3-SCR performance of aged Cu/SAPO-34 s templated by bulky triethylamine (TEA) and tetraethylammonium hydroxide (TEAOH) was mostly recovered, while aged Cu-SAPO-34 templated by small morpholine (MOR) only regained part of its activity [29]. Briend et al. reported that compared with SAPO-34 (MOR), SAPO-34 (TEAOH), with fewer Si-OH-Al bonds and more Si islands, had higher stability [30]. However, Lin et al. demonstrated that the Cu-SAPO-34 (TEA template) with fewer Si islands showed better moisture stability than Cu-SAPO-34 (TEAOH template) with more Si islands [31]. The effect of Si environments on the moisture stability of Cu-SAPO-34 is still unclear and deserves further investigation.

Here, SAPO-34s with different Si content (Si environment) but approximate acid concentrations were synthesized to explore the influence of Si environments on the NH_3-SCR performance and moisture stability of Cu-SAPO-34 catalysts. Bulky TEAOH was chosen as a template for the synthesis of SAPO-34, because large-molecule amines have been evidenced to produce SAPO-34 with better moisture stability than small ones [29,30]. This is owing to the relatively low charge density of bulky amines, which limits the maximum number of $[Si–O–Al]^-$ (corresponding to BAS) in the framework and abates the structural sensitivity upon exposure to moisture. It is demonstrated that the resultant Cu-SAPO-34 with low Si content and abundant Si(4Al) species possesses both excellent NH_3-SCR performance and robust resistance to hydration treatment.

2. Experimental

2.1. Preparation of Cu-SAPO-34 catalysts

TEAOH (35 wt%, Runjing Chemical) was utilized as a template. The Al source, Si source, and P source were pseudoboehmite (68.6 wt% Al_2O_3, Shandong Chemical Company), fumed silica (Qindao Meigao Company), and H_3PO_4 (85 wt%, Tianjin Kemiou Chemical Reagent Company), respectively. No further purification was applied for chemical reagents.

SAPO-34s were hydrothermally synthesized from an initial gel with molar composition 2.0 TEAOH:x SiO_2 :1.0 Al_2O_3:1.0 P_2O_5:50 H_2O (x = 0.3, 0.4, 0.6, and 0.8). First, 17.94 g of H_3PO_4 was poured into the beaker with 25 g of H_2O; then, 11.40 g of pseudoboehmite was added into the H_3PO_4 solution. After stirring for 3 h, the desired amount of fumed silica and 65.47 g of TEAOH solution were added into the above mixture under stirring. The final gel was then transferred to a 150-mL autoclave and heated to 200 °C. The crystallization process lasted for 24 h. The product was recovered by a centrifugation–washing cycle and dried overnight at 110 °C.

Cu-SAPO-34 catalysts with similar Cu content were prepared by a direct ion exchange method reported by us recently [32]. SAPO-34 (5 g) was added to 100 g of $Cu(CH_3COO)_2$ solution (0.015 M−0.02 M) and stirred in a water bath for 3 h (65 °C). After that, the obtained solid was filtered, rinsed with deionized H_2O, dried overnight, and calcined at 600 °C for 6 h. The Cu loading was ca. 1.85 wt % (measured by X-ray fluorescence (XRF), as listed in Table 1 in Section 3.1.1). The catalysts were named Si–X (X is the mole percentage of Si over SAPO-34).

The low-temperature moisture stability of Cu-SAPO-34 catalysts was investigated by a cyclic hydration method developed by us [24]. The calcined catalyst was first treated under 10 vol% H_2O/N_2 (253.4 mL/min) at 80 °C for 30 min, and then heated to 600 °C in dry airflow immediately. The hydration treatment was repeated six times. The treated sample was denoted as Si-X-LH (X is the mole percentage of Si in SAPO-34).

2.2. Activity test

The catalytic activity was measured on a fixed-bed quartz reactor as in our previous report [24]. During each test, 60 mg of sample diluted with 240 mg of quartz pellet was loaded. The reaction gases were 500 ppm of NH_3, 500 ppm of NO, 6.1% O_2, 6.4% H_2O, and balanced with N_2. The gas hourly space velocity (GHSV) was 300,000 h^{-1} (320 mL/min of gas flow). Before the activity test, the sample was preactivated by reaction gases at 553 °C for 120 min. Activity evaluation was conducted from 150 to 500 °C. The inlet and outlet concentrations of NO_x (NO, NO_2, and N_2O) were measured with an FTIR spectrometer (Tensor 27, Bruker) equipped with a 2-m gas cell. The NO_x conversion was calculated as follows:

$$NO_x\text{conversion}(\%) = \frac{([NO]_{in} - [NO]_{out} - [NO_2]_{out} - 2[N_2O]_{out})}{[NO]_{in}} \times 100\% \quad (1)$$

2.3. Kinetic test

The turnover frequencies (TOF) of the Cu-SAPO-34 catalyst were tested in a quartz reactor. Our previous study indicated that the effect of diffusion limitation in this test system on the reaction rate of Cu-SAPO-34 can be removed under the conditions of 900 mL/min and 60–80 mesh [24]. Catalyst (16.5 mg) and 300 mg of quartz pellet (60–80 mesh) were blended and packed

Table 1
Elemental compositions and textural information for the Cu-SAPO-34 catalysts before and after hydration treatment.

Sample	Composition of SAPO-34[a]	Cu content (wt.%)[a]	Isolated Cu^{2+} ions (wt.%)[b]	S_{micro} (m^2/g)[c]	S_{exter} (m^2/g)	V_{micro} (mL/g)[c]	V_{meso} (mL/g)
Si-7.7	$Si_{0.077}Al_{0.497}P_{0.426}O_2$	1.86	0.83	570	33	0.24	0.08
Si-10	$Si_{0.101}Al_{0.490}P_{0.407}O_2$	1.90	1.03	597	38	0.25	0.07
Si-15	$Si_{0.150}Al_{0.483}P_{0.366}O_2$	1.85	1.03	511	46	0.22	0.07
Si-20	$Si_{0.204}Al_{0.443}P_{0.353}O_2$	1.82	1.03	515	58	0.22	0.10
Si-7.7-LH	–	–	1.11	530	25	0.23	0.05
Si-10-LH	–	–	1.25	513	45	0.21	0.07
Si-15-LH	–	–	1.30	420	47	0.21	0.07
Si-20-LH	–	–	1.21	398	38	0.18	0.07

[a] Measured by XRF.
[b] Quantified by EPR.
[c] Determined by *t*-plot method.

in the reactor. Gases composed of 500 ppm NH_3, 500 ppm NO, 6.1% O_2, and 3.6% H_2O (balanced with N_2) were applied here. The flow rate was 900 mL/min, corresponding to a GHSV of 3,270,000 h^{-1}. The testing procedure was the same as in the above catalytic activity test. Activity evaluation was conducted from 150 to 210 °C at an interval of 20 °C to ensure the NO_x conversion $\leq$ 20%. The TOF was calculated as follows:

$$\mathrm{TOF} = \frac{\mathrm{NO}_x\mathrm{conversion}(\%) \times [\mathrm{C}] \times F \times 63.5}{w \times m \times 22.4}\left(\mathrm{s}^{-1}\right) \quad (2)$$

Here, w is mass fraction of *iso*-Cu^{2+} ions, F is 900 mL/min, [C] is 500 ppm, and m is 0.0165 g.

2.4. Characterization

The chemical composition of the sample was determined with XRF (PANalytical). Thermogravimetry (TG) analysis was performed on a TA SDTQ600 analyzer with a temperature-programmed rate of 10 °C/min under an air flow of 100 mL/min. The morphology and size of the crystals were determined by scanning electron microscopy (SEM) on a Hitachi SU8020 microscope. The ASAP 2020 automatic surface analyzer system was applied to test the textural properties of the samples (Micromeritics) at 77 K. The sample was degassed at 350 °C for 6 h prior to the analysis. The structural properties of the samples were recorded through a PANalytical X'Pert Pro diffractometer with Cu radiation (λ = 0.15406 nm). A Varian Infinity-plus 400 spectrometer equipped with a 5-mm MAS probe (spinning rate 8 kHz) was applied to confirm the Si coordination, and the resonance frequency was 79.4 MHz. Kaolinite was applied to calibrated the chemical shift of ^{29}Si. The content of *iso*-Cu^{2+} ions over Cu-SAPO-34 was determined with EPR spectra on a Bruker A200 at 110 K. Before the test, the sample was calcined in air at 600 °C. After cooling in air to room temperature, the sample was placed into a glass tube and then heated to 120 °C. Dry N_2 was purged into the tube to remove H_2O in the sample, and the quantitative results were calibrated by the standard $CuSO_4$ solution. A chemisorption analyzer (AutoChem II, Micromeritics) with a thermal conductivity detector was used to characterize the H_2-TPR and NH_3-TPD of the catalysts. For H_2-TPR, 100 mg of the sample was pretreated for 1 h in 2% O_2/He (30 mL/min) at 500 °C. After the sample was cooled to 100 °C, the gas was switched to Ar and held for 10 min to remove the O_2 in the gas line. Then 10% H_2/Ar (30 mL/min) was introduced and the H_2-TPR was carried out at a heating rate of 10 °C/min from 100 to 800 °C. In situ and ex situ DRIFTS were collected by accumulating 64 scans at a resolution of 4 cm^{-1} over a TENSOR 27 (Bruker) equipped with a mercury cadmium telluride detector and a high-temperature chamber with ZnSe windows. Before the collection of the spectrum, the sample was purged with N_2 at 500 °C to remove the absorbed impurities. The spectrum of KBr was applied as a background for ex situ DRIFTS measurements, and the spectrum of the sample under the same conditions was applied as the background for in situ DRIFTS. For the NH_3-TPD experiment, a detailed procedure can be found in our previous study [28]. The reactivity of NH_3 adsorbed on BAS with NO/O_2 was determined at 250 °C. First, a pretreatment with 500 ppm of NH_3/N_2 (24 mL/min) for 40 min at 250 °C and a subsequent purge with N_2 (20 mL/min) for 20 min were carried out to prepare the catalyst with preadsorbed NH_3. NO/N_2 (500 ppm) and 6.3% O_2/N_2 (36 mL/min) were then introduced into the reaction chamber and the DRIFT spectra were collected simultaneously at an interval of 2 min. Afterward, NO/O_2 reactant gas was switched immediately to N_2 gas . After further treatment with N_2 for 20 min, DRIFTS of TPD were collected after holding for 30 min at a certain temperature (250, 300, 350, and 400 °C).

3. Results and discussion

3.1. The effect of Si environments on the NH_3 selective catalytic reduction performance of Cu-SAPO-34 s

3.1.1. Composition, textural properties, and morphology

Four Cu-SAPO-34 samples with incremental Si content from 7.7 to 20.4 mol% and similar Cu loadings (1.82–1.90 wt%) were prepared for the study (Table 1). N_2 adsorption–desorption analysis was used to determine the textural properties of the fresh samples. As listed in Table 1, the micropore surface areas and micropore volumes of all the samples are greater than 500 m^2/g and 0.22 mL/g respectively, suggesting their high crystallinity [33]. The XRD patterns of the samples are displayed in Fig. A1, which presents typical patterns of CHA structure. No diffraction peaks due to Cu_xO_y could be identified, indicating that Cu species are highly dispersed. The SEM images of the catalysts are presented in Fig. 1, which shows a typical rhombohedral morphology for SAPO-34. A gradual decline in crystal size (from ~ 600 to 200 nm) could be observed following the increase of Si content. This variation trend may be explained by the alteration of the Si coordination environments of the samples (see the ^{29}Si MAS NMR results in Section 3.1.4), because they affect the angle/length of the T–O–T bonds and thus the crystallization and crystal size. In effect, it has been proposed by the previous literature that the crystallization process could be terminated due to the presence of growth limitations dictated by the T–O–T bond angle/length [34].

3.1.2. Active sites and reducibility of Cu^{2+} ions

EPR was applied to determine the content of isolated Cu^{2+} ions (*iso*-Cu^{2+}) and their location over Cu-SAPO-34. The EPR spectra are shown in Fig. A2a. The parallel g-values of all the catalysts are identical ($g_{//}$ = 2.36), indicating the similar locations of *iso*-Cu^{2+} ions under the six-membered ring sites [10]. From Table 1, it can be

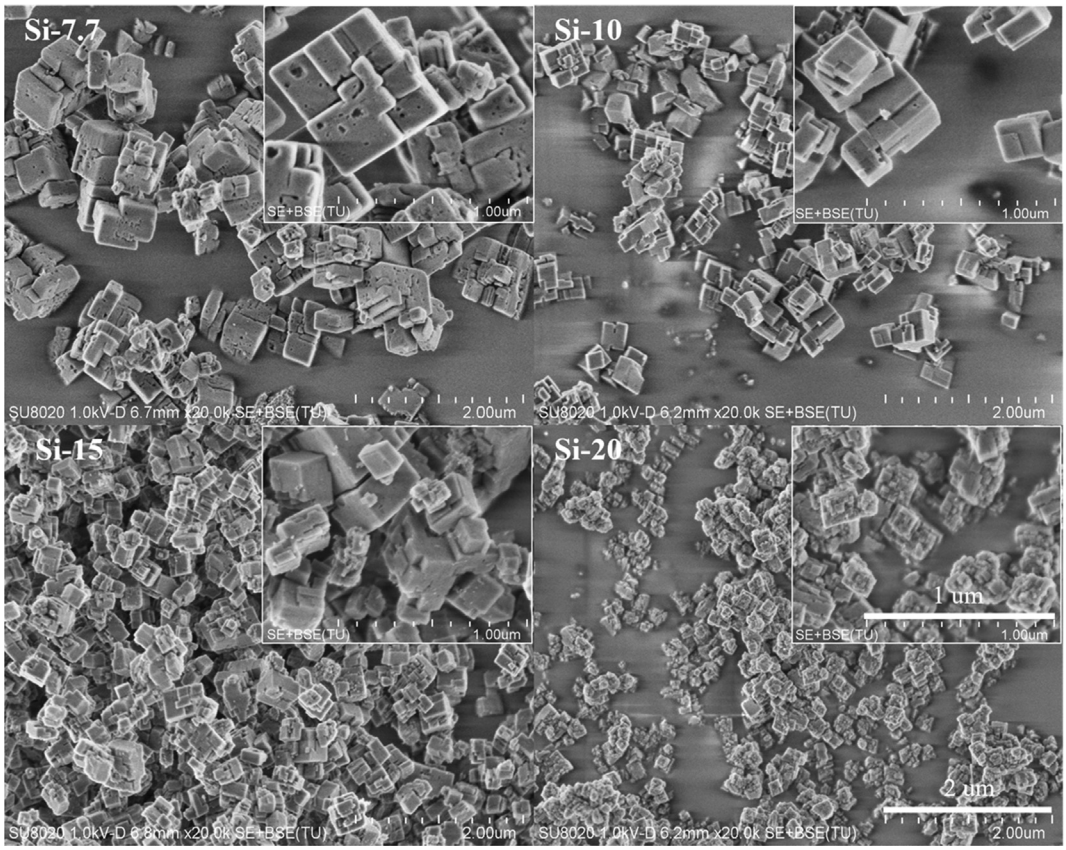

Fig. 1. The SEM images of the Cu-SAPO-34 catalysts.

seen that only part of the Cu species exists as *iso*-Cu^{2+} ions (ca. 50% of total Cu loadings); the contents of *iso*-Cu^{2+} ions on Cu-SAPO-34 s are rather similar (1.03 wt%), except in sample Si-7.7 (0.83 wt%).

H_2–TPR was employed to identify the copper species on the Cu-SAPO-34 catalysts and determine their reducibility (Fig. 2a). Only one type of *iso*-Cu^{2+} ions exists over Cu-SAPO-34 revealed by EPR, and the reduction temperature of Cu^{2+} species is always lower than 350 °C [24,35–37]. The three former peaks located at around 200, 270, and 400 °C are ascribed to the continuous reduction of highly dispersed surface CuO to Cu^0 [35,38], Cu^{2+} ions to Cu^+ ions [28,39–41], and bulk CuO to Cu^0 [42,43]. The peak at the temperature above 515 °C is owing to the further reduction of Cu^+ to Cu^0 [24,28,39]. The H_2 consumption for Cu species is calculated and shown in Table A1. It is found that the H_2/Cu ratio for all samples is less than 1, especially for the high-Si samples Si-15 and Si-20 (less than 0.5). As the reduction peak of Cu^+ ions is less conspicuous on Si-15 and Si-20, it is assumed that there exist large amounts of nonreducible Cu^+ ions on the samples. The formation of Cu^+ probably includes the contributions of the reduction of isolated Cu^{2+} and the originally existing Cu^+ in the catalysts (possibly

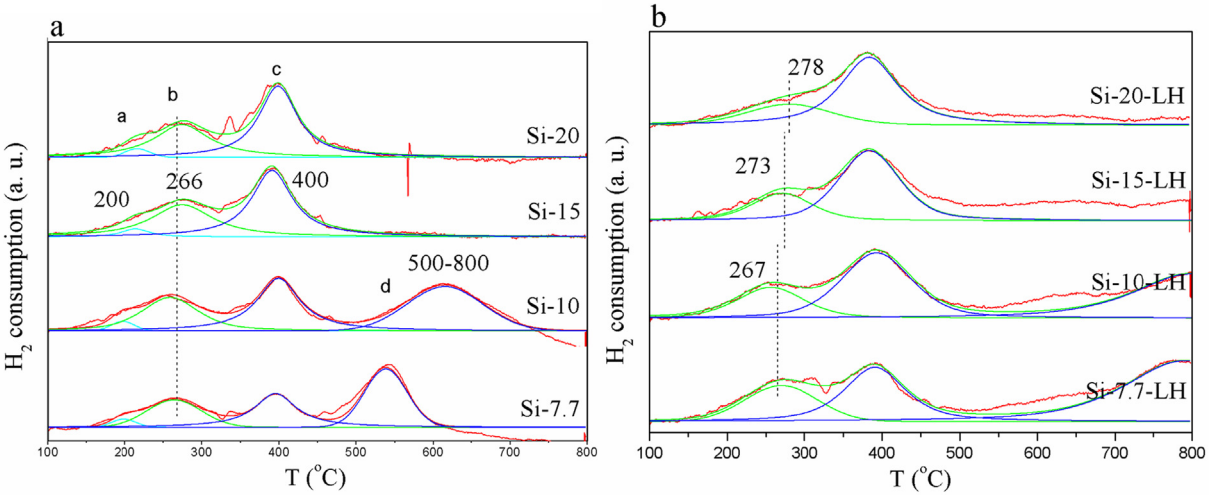

Fig. 2. The H_2-TPR profiles of Cu-SAPO-34 catalysts before (a) and after (b) hydration treatment.

formed during the pretreatment process) [10,11,44]. Moreover, the Cu^+ reduction peak moves to high temperature from Si-7.7 to Si-20, while the reduction temperature of isolated Cu^{2+} is adjacent for all the samples. Given that the acid strength of the carriers intensifies with the increment of Si content (see Section 3.1.3), the framework negativity of the carriers is speculated to have an increasing trend, and thus enhance interactions between Cu^+ ions and the negative framework. This would suppress the reduction of Cu^+ to Cu, leading to the high-temperature movement of the reduction peak following the increase in Si content.

3.1.3. Acid properties

The DRIFTS spectra (OH region) of Cu-SAPO-34 are shown in Fig. 3a. From 3500 to 3800 cm^{-1}, five peaks centered around 3791, 3740, 3672, 3619, and 3596 cm^{-1} are discerned, which are assigned to the OH stretching vibrations of Al–OH, Si–OH, P–OH, and Si–OH–Al bridge hydroxyls located in the 8MR channels and the D6Rs, respectively [17,45–47]. Notably, the band intensity of 3740 cm^{-1} augments in parallel with the Si content, suggesting an increase of silanol groups on the surface. The relative amounts of the Si–OH–Al hydroxyls are calculated according to the integrated band areas in the range 3550–3660 cm^{-1} (Table 2), indicating that all the samples possess similar amounts of BAS.

The desorption processes of adsorbed NH_3 over the Cu-SAPO-34 s are followed by DRIFT spectroscopy (Fig. A3). Similar desorption behavior can be observed for all the samples. The band at 3675 cm^{-1} is evidently reduced from 150 to 200 °C, suggesting the preferential desorption of NH_3 from P–OH. Above 200 °C, a gradual recovery of both the BAS and LAS could be observed, as evidenced by the decline of the bands at 3625, 3600, 1485, and 1601 cm^{-1}. The existence of a small number of LAS (weak band at 1601 cm^{-1}) in Cu-SAPO-34 should mainly originate from *iso*-Cu^{2+} ions [9]. With the temperature further increasing to 300 °C, the band at 1601 cm^{-1} disappears, showing the complete desorption of NH_3 from LAS. Meanwhile, the intensities of the bands around 3625, 3600, and 1485 cm^{-1} continue to decline until 400 °C, corresponding to the recovery of the BAS with higher strength. Fig. 3b presents the normalized areas of Si–OH–Al bonds (3550–3660 cm^{-1}) at different desorption temperatures. Clearly, NH_3 desorption at higher temperatures is more prominent on the samples with higher Si content, and the ratio of strong BAS has the following trend: Si-7.7 < Si-10 < Si-15 < Si-20.

NH_3-TPD was also employed to quantify the acidity of the catalysts. From Fig. 3c, one desorption peak centered at around 400 °C and a shoulder at 300 °C could be discerned. According to the DRIFTS of NH_3-TPD results, the peak at 300 °C can be ascribed to NH_3 desorption from LAS and BAS with moderate acid strength, while the peak at ca. 400 °C is attributed to further NH_3 desorption from stronger BAS. Clearly, Cu-SAPO-34 with higher Si content has greater acid strength (higher NH_3 desorption temperature), which is consistent with the acid strength order derived from NH_3-TPD DRIFTS. The total acid amounts are calculated according to the NH_3-TPD curves. As shown in Table 2, all the samples possess similar acid amounts.

These results demonstrate that the increment of Si content only affects the acid strength, but does not alter the BAS or the total acid amount of Cu-SAPO-34 synthesized by the bulky TEAOH template. Given the identical TEA^+ number in each CHA cage for all the samples (Table 2), this phenomenon is not surprising, since it is the incorporated organic template (positive charge) that actually governs the maximum amount of $[Si–O–Al]^-$ (the number of BAS) in the framework.

3.1.4. The distribution of Si species over Cu-SAPO-34 catalysts

^{29}Si MAS NMR was applied to identify the variation of Si environments over Cu-SAPO-34 with the increase of Si content. As

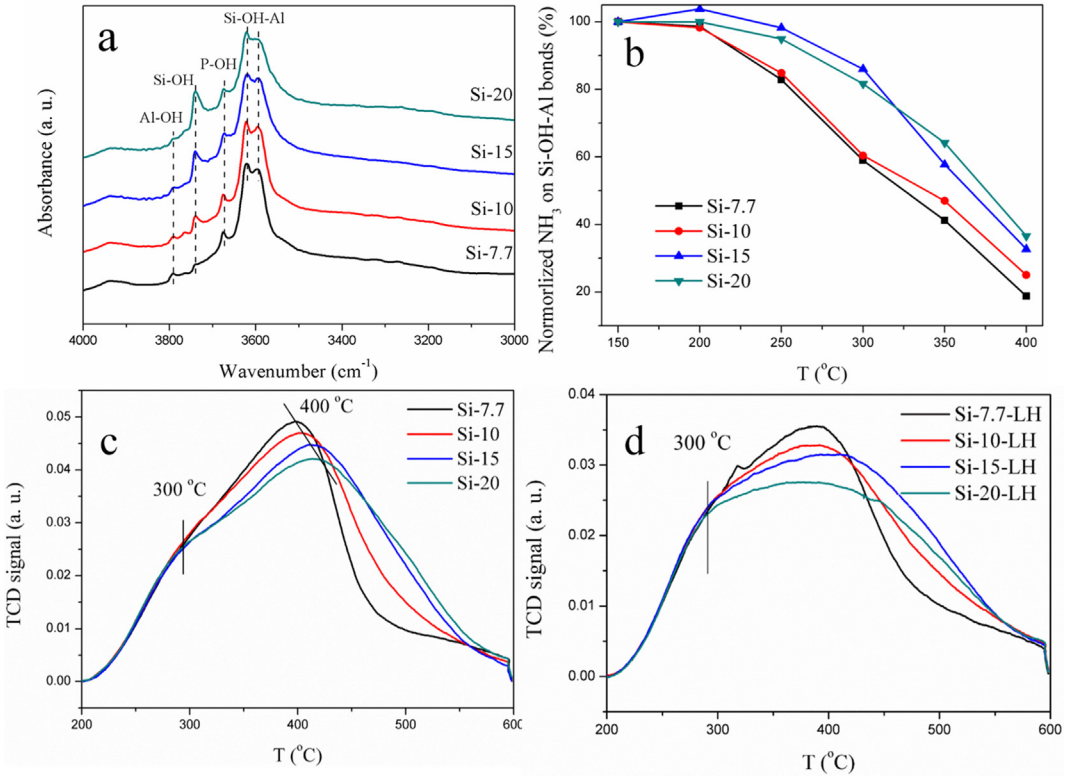

Fig. 3. The acidity of Cu-SAPO-34 catalysts before and after hydration treatment. (a) DRIFTS spectra (OH region); (b) normalized DRIFTS areas of NH_3 on acidic hydroxyls (3550–3660 cm^{-1}) during the NH_3 TPD process; (c, d) NH_3 TPD curves. Fresh Cu-SAPO-34 s for a, b, and c and hydrated catalyst for d.

Table 2
The acid properties of the Cu-SAPO-34 catalysts before and after hydration treatment.

Sample	Normalized BAS (%)[a]	Total acid sites (mmol/g)[b]	Number of TEA^+ per CHA cage[c]	Sample	Total acid sites (mmol/g)[b]	Decreasing degree (%)[d]
Si-7.7	91.4	1.13	1	Si-7.7-LH	0.96	15.0
Si-10	95.2	1.22	1	Si-10-LH	1.01	17.2
Si-15	100	1.23	1	Si-15-LH	1.01	17.9
Si-20	99.0	1.23	1	Si-20-LH	0.95	22.7

[a] Normalized BAS by integrating the area of the acidic hydroxyls band (3550 to 3660 cm^{-1}).
[b] Determined by NH_3-TPD.
[c] Calculated according to TG and XRF.
[d] The loss of total acid sites after hydration treatment.

shown in Fig. 4, the ^{29}Si MAS NMR spectra present five peaks at −91.87, −95.35, −100.26, −105.5, and −110.23 ppm, which are ascribed to Si(4Al), Si(3Al), Si(2Al), Si(1Al), and Si(0Al) species, respectively [19]. It has previously been demonstrated that the order of acid strength of different Si environments in SAPOs is Si(4Al) < Si(3Al) < Si(2Al) < Si(1Al) [20]. The deconvoluted results shown in Table A2 reveal that the ratio of Si islands (Si(*n*Al), *n* = 0–3) rises with the increment of Si content, yet the ratio of Si (4Al) presents an opposite trend, suggesting higher acid strength of the sample with higher Si content. This is in good congruence with the acidity variation evidenced by NH_3-TPD DRIFT.

3.1.5. Reactivity of NH_3 preadsorbed on the Brønsted acid sites of Cu-SAPO-34

In situ DRIFT spectroscopy was conducted to explore the correlation between the BAS strength and the NH_3-SCR performance based on the fresh sample of Si-20. The areas of the bands in the range 3550–3660 cm^{-1} were employed to evaluate the quantity of NH_3 adsorbed on BAS, and the normalized results are shown in Fig. 5. From Fig. 5a, the preadsorbed NH_3 on BAS diminishes gradually with the introduction of NO, but the consumption rate slows down with the reaction time, implying inhomogeneous activity of adsorbed NH_3 on BAS. The residual NH_3 species after reaction were further studied by DRIFTS of TPD. As shown in Fig. 5b, with the temperature rising from 250 to 350 °C, no release of NH_3 was detected. On further increase to 400 °C, a certain amount of NH_3 was desorbed. The results imply that the NH_3 adsorbed onto weaker BAS (associated with Si(4Al) species) was preferentially consumed during the reaction. Moreover, the NO reaction with preadsorbed NH_3 over the low-silica sample Si-7.7 was also investigated and the results are displayed in Fig. A4. It is found that the NH_3 consumption rate on Si-7.7 is higher than that on Si-20 in the first 15 min, which confirms the higher reactivity of NH_3 adsorbed on mild BAS. Paolucci et al. confirmed that the formation of Cu^{2+} dimers is the rate limitation step during the NH_3-SCR process, and the existence of NH_3 would facilitate the mobility of Cu ions by the generation of $Cu^+[NH_3]_2$ ions [48]. Wang et al. reported that the BAS supplies NH_3 via migration to Cu ions for SCR reaction [15]. Thus, it is reasonable to see the preferential consumption of NH_3 on moderate BAS (associated with Si(4Al) species) due to its higher mobility than on strong BAS (associated with Si islands).

3.1.6. NH_3 selective catalytic reduction performance and kinetic study

Fig. 6 and Fig. A5 display the TOFs and apparent activation energy (E_a) values of the catalysts. It can be observed that the TOFs of Cu-SAPO-34 catalysts decline in the order Si-7.7 > Si-10 > Si-15 > Si-20. The derived E_a values of the catalysts have the opposite trend, indicating an enhanced activation barrier with increased Si content. As revealed by the above characterizations, the differences among the four catalysts mainly lie in the Si environments (acid strength) and crystal sizes. Given that Shen's group has evidenced that the SCR reaction rate of Cu-CHA catalysts is not affected by crystal size [25,49], here the distinct Si environments of the catalysts are considered to be responsible for the variations of the E_a and the NH_3-SCR performance. As Section 3.1.5 has demonstrated that NH_3 adsorbed onto mild BAS (associated with Si(4Al) species) has higher activity, it is concluded that Si(4Al)-enriched low-Si Cu-SAPO-34 templated by bulky amines has better catalytic performance for the NH_3-SCR reaction.

3.2. The effect of Si environments on the moisture stability of Cu-SAPO-34 catalysts

3.2.1. The variations of textural properties, acidity, and Si environments

The XRD patterns of the hydrated samples (Si-X-LH) are given in Fig. A1b, which presents typical diffraction peaks of CHA structure except for reduced crystallinity. The textural properties of the hydrated samples displayed in Table 1 show a decrease in micropore area and micropore volume as compared with those of the fresh ones. The loss intensifies following the increase in Si content. More specifically, the decline in micropore area for Si-7.7, Si-10, Si-15, and Si-20 upon hydration treatment is 7.0, 14.1, 17.8, and 22.7%, respectively.

Fig. 3d illustrates the NH_3-TPD profiles of the hydrated catalysts. The high-temperature peak ascribed to strong BAS is smaller than that of the corresponding fresh catalyst. The quantified results are listed in Table 2. It can be seen that the decay of total acid sites is proportional to the increment of Si content and consistent with the decrease in textural properties.

Fig. 4b shows the ^{29}Si MAS NMR spectra of the hydrated catalysts. The deconvoluted results are displayed in Table A2. The proportions of Si island species evidently increase upon hydration treatment, whereas the Si(4Al) species decreases. More specifically, for hydrated sample Si-7.7, the disappeared Si(4Al) species were mainly transferred to Si(3Al); for hydrated Si-10, Si-15, and Si-20, the proportions of Si(*n*Al) (*n* = 0–2) species showed more obvious increase at the expense of Si(4Al). In addition, defect Si species located from −75 to −85 ppm were observed for hydrated samples, which resulted from the hydrolysis of Si–O–Al bonds. These changes imply that Si(4Al) species can migrate and lead to the formation of larger Si islands during the hydration treatment. It is well known that the average BAS per Si atom in the Si islands (less than1) are lower than the average Si(4Al) species (=1) [20]; the larger the Si islands, the smaller the average BAS per Si atom (the Si (0Al) species do not even generate acid sites). Thus, it is reasonable to see the increasing decay of total acid amount from hydrated Si-7.7 to Si-20. The change of the Si environments of the hydrated catalysts can be understood from the spatial distance between Si atoms (Fig. A6): with the increment of Si content, the spatial distance between Si atoms decreases, which facilitates the migration and aggregation of Si atoms and thus the growth of Si islands.

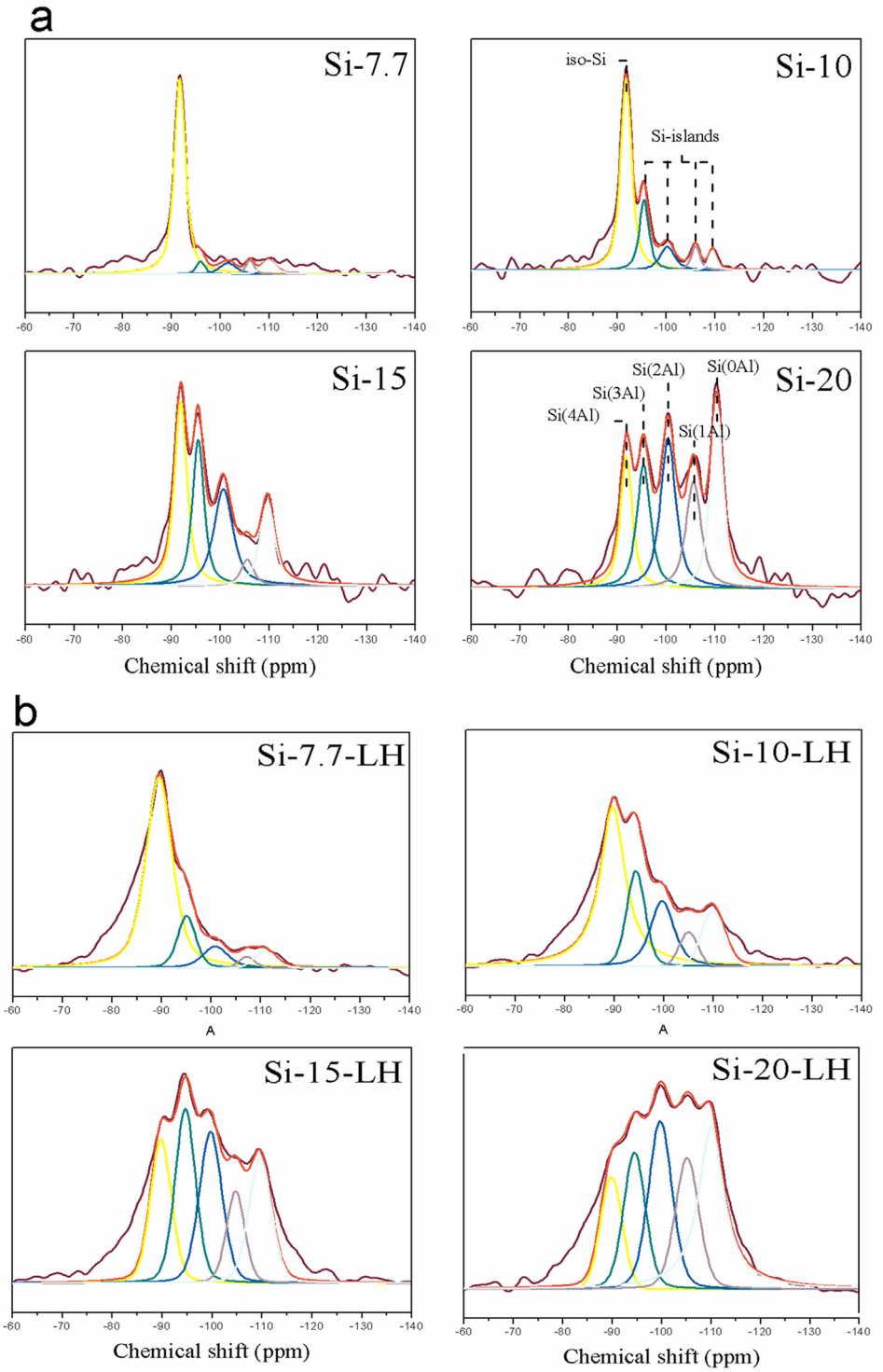

Fig. 4. The ^{29}Si MAS NMR spectra of the Cu-SAPO-34 catalysts before (a) and after (b) hydration treatment.

3.2.2. The variations of active sites

The H_2-TPR profiles of the hydrated catalysts are presented in Fig. 2b. The change in reduction peaks should result from the change in carrier properties that affect the interactions between Cu species and the framework [39]. Given that the main difference between the carriers lies in the Si environments, the high-temperature shift of the reduction peak of Cu^+ to Cu^0 after hydration is ascribed to the increment of Si islands (acid strength). In addition, the reduction temperature of *iso*-Cu^{2+} ions (~270 °C) shows a slight high-temperature shift following the increment of Si content, implying decreased reducibility of *iso*-Cu^{2+} ions. This would be unfavorable for NH_3-SCR performance [24,28].

EPR was also utilized to quantify the variation of *iso*-Cu^{2+} ion content over the hydrated catalysts (Fig. A2b). The *g*-value and *A*-value of the hyperfine structure of Cu^{2+} ions ($g_{//}$ = 2.36 and *A* = 140) are found to be the same as those of the fresh ones, indicating the unchanged coordination environment of *iso*-Cu^{2+} ions. From the quantified results listed in Table 1, the numbers of

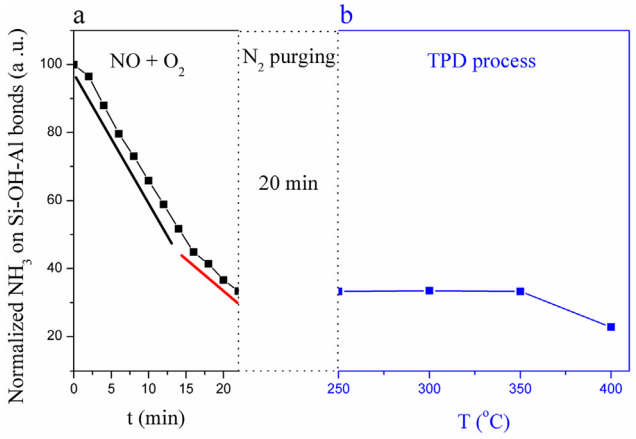

Fig. 5. Normalized DRIFTS areas of NH_3 on Si–OH–Al bonds (3550–3660 cm^{-1}). (a) NO reaction with preadsorbed NH_3 over the fresh sample Si-20 at 250 °C for 22 min; (b) the subsequent TPD process from 250 to 400 °C after purging with N_2 for 20 min after (a).

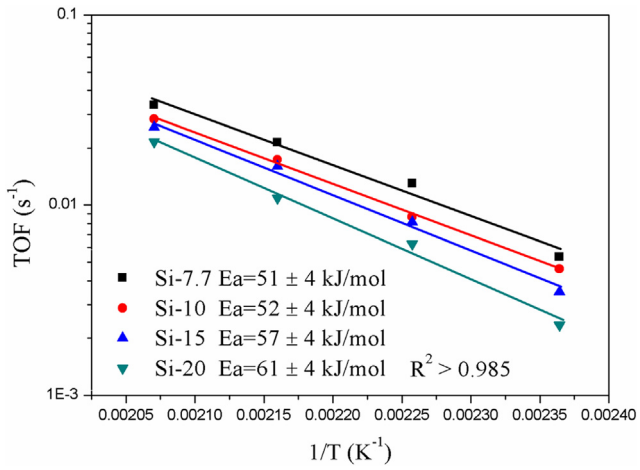

Fig. 6. TOFs of the fresh Cu-SAPO-34 catalysts at different temperatures. GHSV: 3,270,000 h^{-1}.

iso-Cu^{2+} ions show a slight increase after hydration. However, considering that the *iso*-Cu^{2+} contents on the hydrated samples resemble each other, the impact of the incremental *iso*-Cu^{2+} ions on the NH_3-SCR performance should be similar.

3.2.3. The variations in NH_3 selective catalytic reduction activity

Fig. 7 presents the activity results for the catalysts. All the fresh catalysts exhibit prominent NH_3-SCR performance (Fig. 7a), showing a broad temperature window of 250–500 °C with NO_x conversion above 90% (T_{90}). For the low-Si catalysts Si-7.7 and Si-10.0, the temperature window is even broader (200–500 °C). The low-temperature SCR performance of the fresh catalysts has the order Si-7.7 ~ Si-10 > Si-15 > Si-20, similarly to the order of TOFs obtained in Section 3.1.6. The content of *iso*-Cu^{2+} ions on Si-10 is slightly higher than that on Si-7.7, which may help Si-10 display low-temperature NO_x conversions comparable to those on Si-7.7. The relatively low NO_x conversion on Si-7.7 at high temperature may result from its lower acid strength, which is unfavorable to the absorption of NH_3 at high temperature. The nonadsorbed NH_3 would be consumed by O_2 instead of NO [50], leading to an apparently decreased NO_x conversion. The formation of N_2O is extremely low during the reaction (less than3 ppm; data are not listed here), indicating high N_2 selectivity on all catalysts.

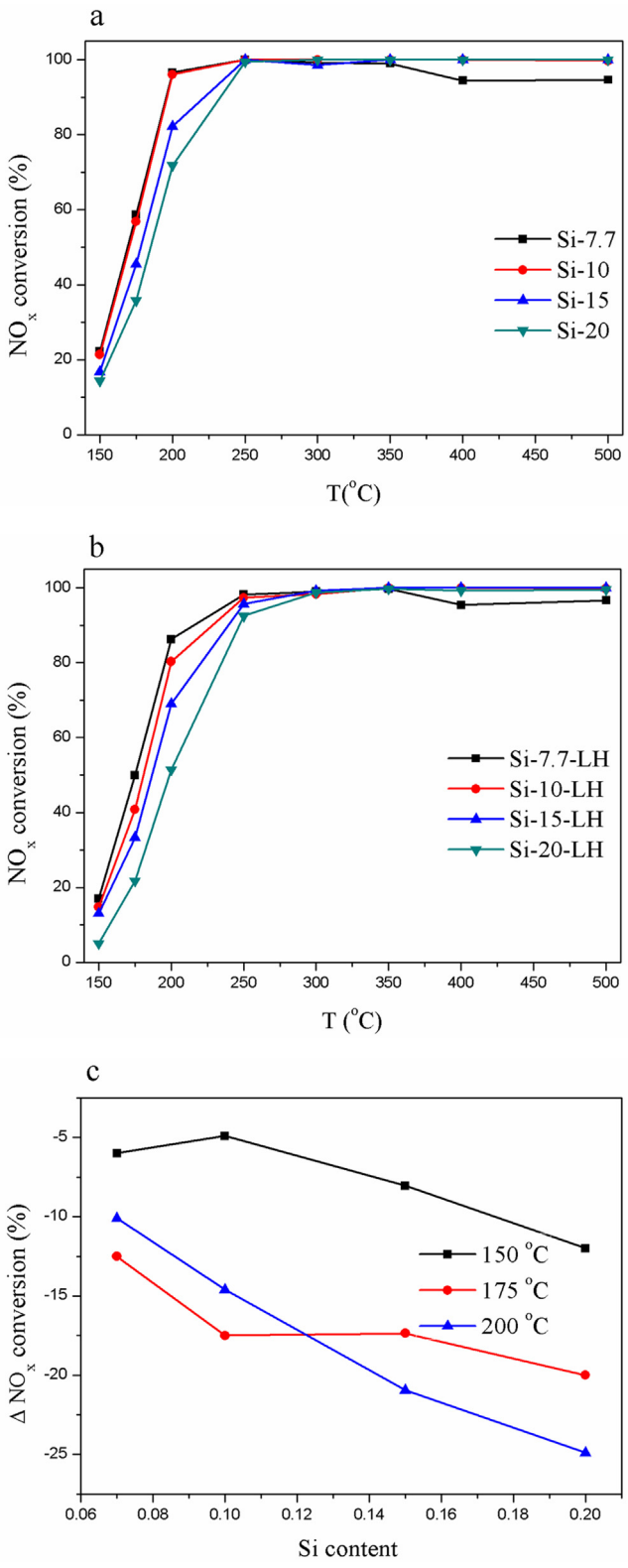

Fig. 7. The NH_3-SCR performance of Cu-SAPO-34 catalysts before (a) and after (b) hydration treatment. The variation of NO_x conversion on Cu-SAPO-34 catalysts upon hydration treatment (c). ΔNO_x conversion = NO_x $conversion_{hydrated\ catalyst}$ − NO_x $conversion_{fresh\ catalyst}$. GHSV: 300,000 h^{-1}.

After six cycles of hydration treatment, the activity in the low-temperature range decreases for all catalysts, although the high-temperature activity is less changed (Fig. 7b). The

low-temperature SCR performance of the hydrated catalysts has an order similar to that for the fresh catalysts. For clear comparison, the variations of low-temperature NO_x conversion before and after the treatment are plotted and displayed in Fig. 7c. It is found that the activity loss intensifies from catalyst Si-7.7 to Si-20. As the above characterizations have demonstrated that upon hydration treatment, the textural properties, the acid sites, and the reducibility of *iso*-Cu^{2+} ions decrease gradually from catalyst Si-7.7 to Si-20, it is reasonable to see the same declining trend of SCR activity.

The main differences among the catalysts lie in Si content (Si environment) and crystal size. Regarding the influence of crystal size on moisture stability, Huang et al. recently reported that the Cu-SAPO-34 catalysts with smaller crystal size had better low-temperature hydrothermal stability [25]. Moreover, the difference in crystal size among the catalysts is not huge (from 200 to 600 nm). For Si-10 and Si-15 with approximate crystal sizes, the former shows better preserved physicochemical properties and NH_3-SCR performance. We thus speculate that the decay of the catalysts in physicochemical and catalytic properties mainly results from their distinct Si environments. The catalyst with higher content of Si islands is more sensitive to hydration treatment due to the easier occurrence of Si migration, which leads to the formation of larger Si islands (corresponding to more loss of acid sites and stronger acidity) and thus worse NH_3-SCR performance at low temperatures. It is believed that Cu-SAPO-34, with lower Si content and abundant Si(4Al) species (moderate BAS), should be a better candidate for deNO_x application due to its higher resistance to moisture and superior SCR performance.

Finally, to verify our findings about the effect of Si environments on SCR activity and moisture stability, we further prepared Cu-SAPO-34 with varying Si content using bulky triethylamine (TEA) as a template (1 TEA per CHA cage) [51]. Our previous work has demonstrated that the Si(4Al) species dominates in SAPO-34-TEA with Si content of ~ 8.0% and Si islands start to appear with further increasing Si content [52,53]. The NH_3-SCR performance of the catalysts before and after hydration treatment is shown in Fig. A7. It can be seen that the activity of the fresh catalysts has the order of Si-T11.5 < Si-T9.1 ~ Si-T7.7. Meanwhile, Si-T7.7 and Si-T9.1 also possess superior moisture stability (Fig. A7c). The results on Cu-SAPO-34-TEA are consistent with those on Cu-SAPO-34-TEAOH, confirming our conclusions well. In addition, we emphasize here the importance of bulky template for the preparation of robust Cu-SAPO-34 catalyst. As given in Fig. A8, Si (4Al)-rich Cu-SAPO-34 templated by small diethylamine (1.75 DEA per CHA cage) displays terrible moisture stability, despite its excellent fresh SCR activity. This should be caused by its extremely high content of Si(4Al) species (acid concentration), which is, however, hard to decrease due to the high Si incorporation of SAPO-34 templated by small amines [51,54].

4. Conclusions

The impact of Si environments on NO_x conversion and moisture stability has been investigated based on Cu-SAPO-34 catalysts with comparable Cu loadings and *iso*-Cu^{2+} contents. Characterizations demonstrate that with the increase of Si content in Cu-SAPO-34, the BAS amount remains almost unchanged due to there being one template (TEA^+) per CHA cage, which determines the maximum framework charge and the number of BAS; the ratio of Si islands increases at the expense of Si(4Al) species, leading to incremental acid strength. In situ DRIFTS experiments reveal that the NH_3 adsorbed onto moderate BAS (associated with Si(4Al) species) has higher reactivity than that on strong BAS, consistent with the superior NH_3-SCR activity and the low E_a on sample Si-7.7 with the highest amount of Si(4Al) species.

Low-temperature hydration treatment induces a decrease in textural properties, strong BAS, and the reducibility of *iso*-Cu^{2+}. This deterioration intensifies with the incremental Si islands in the catalysts due to the easier occurrence of Si migration and the formation of larger Si islands (more loss of acid sites). Thus, the catalytic activity of the hydrated Cu-SAPO-34s declines with the increase of Si islands content. The excellent SCR performance and robust moisture stability observed for sample Si-7.7 suggest that bulky amine-templated Cu-SAPO-34 catalysts with lower Si content and abundant Si(4Al) species would be promising candidates for deNO_x application.

Declaration of Competing Interest

The authors declare that they have no known competing financial interests or personal relationships that could have appeared to influence the work reported in this paper.

Acknowledgments

The authors thank the National Natural Science Foundation of China (Grants 22006076, 91545104, 21606221, 21676262, 21991090, and 21991091), the China Postdoctoral Science Foundation (Grant 2017M621169), and the Key Research Program of Frontier Sciences, Chinese Academy of Sciences (Grant QYZDB-SSW-JSC040) for financial support.

References

[1] S.C. Anenberg, J. Miller, R. Minjares, L. Du, D.K. Henze, F. Lacey, C.S. Malley, L. Emberson, V. Franco, Z. Klimont, C. Heyes, Impacts and mitigation of excess diesel-related NOx emissions in 11 major vehicle markets, Nature 545 (2017) 467–471.
[2] R. Huang, Y. Zhang, C. Bozzetti, K. Ho, J. Cao, Y. Han, K.R. Daellenbach, J.G. Slowik, S.M. Platt, F. Canonaco, P. Zotter, R. Wolf, S.M. Pieber, E.A. Bruns, M. Crippa, G. Ciarelli, A. Piazzalunga, M. Schwikowski, G. Abbaszade, J. Schnelle Kreis, R. Zimmermann, Z. An, S. Szidat, U. Baltensperger, I.E. Haddad, A.S.H. Prevot, High secondary aerosol contribution to particulate pollution during haze events in China, Nature 514 (2014) 218–222.
[3] J. Wang, H. Zhao, G. Haller, Y. Li, Recent advances in the selective catalytic reduction of NOx with NH3 on Cu-Chabazite catalysts, Appl. Catal. B Environ. 202 (2017) 346–354.
[4] Y. Shan, X. Shi, Z. Yan, J. Liu, Y. Yu, H. He, Deactivation of Cu-SSZ-13 in the presence of SO2 during hydrothermal aging, Catal. Today 320 (2017) 84–90.
[5] M. Xu, J. Wang, T. Yu, J. Wang, M. Shen, New insight into Cu/SAPO-34 preparation procedure: Impact of NH4-SAPO-34 on the structure and Cu distribution in Cu-SAPO-34 NH3-SCR catalysts, Appl. Catal. B Environ. 220 (2018) 161–170.
[6] C. Paolucci, J.R. Di Iorio, F.H. Ribeiro, R. Gounder, W.F. Schneider, Catalysis Science of NOx Selective Catalytic Reduction With Ammonia Over Cu-SSZ-13 and Cu-SAPO-34, in: C. Song (Ed.), Advances in Catalysis, Academic Press, 2016, pp. 1–107.
[7] D.W. Fickel, E. D'Addio, J.A. Lauterbach, R.F. Lobo, The ammonia selective catalytic reduction activity of copper-exchanged small-pore zeolites, Appl. Catal. B Environ. 102 (2011) 441–448.
[8] P.G. Blakeman, E.M. Burkholder, H.-Y. Chen, J.E. Collier, J.M. Fedeyko, H. Jobson, R.R. Rajaram, The role of pore size on the thermal stability of zeolite supported Cu SCR catalysts, Catal. Today 231 (2014) 56–63.
[9] L. Wang, W. Li, G. Qi, D. Weng, Location and nature of Cu species in Cu/SAPO-34 for selective catalytic reduction of NO with NH3, J. Catal. 289 (2012) 21–29.
[10] J. Xue, X. Wang, G. Qi, J. Wang, M. Shen, W. Li, Characterization of copper species over Cu/SAPO-34 in selective catalytic reduction of NOx with ammonia: Relationships between active Cu sites and de-NOx performance at low temperature, J. Catal. 297 (2013) 56–64.
[11] J. Wang, T. Yu, X. Wang, G. Qi, J. Xue, M. Shen, W. Li, The influence of silicon on the catalytic properties of Cu/SAPO-34 for NOx reduction by ammonia-SCR, Appl. Catal. B Environ. 127 (2012) 137–147.
[12] C. Petitto, G. Delahay, Selective catalytic reduction of NOx by NH3 on Cu-SAPO-34 catalysts: Influence of silicium content on the activity of calcined and hydrotreated samples, Chem. Eng. J. 264 (2015) 404–410.
[13] T. Yu, D. Fan, T. Hao, J. Wang, M. Shen, W. Li, The effect of various templates on the NH3-SCR activities over Cu/SAPO-34 catalysts, Chem. Eng. J. 243 (2014) 159–168.
[14] T. Yu, J. Wang, M. Shen, W. Li, NH3-SCR over Cu/SAPO-34 catalysts with various acid contents and low Cu loading, Catal. Sci. Technol. 3 (2013) 3234–3241.

[15] D. Wang, L. Zhang, K. Kamasamudram, W.S. Epling, In Situ-DRIFTS Study of Selective Catalytic Reduction of NOx by NH3 over Cu-Exchanged SAPO-34, ACS Catal. 3 (2013) 871–881.
[16] W. Su, H. Chang, Y. Peng, C. Zhang, J. Li, Reaction Pathway Investigation on the Selective Catalytic Reduction of NO with NH3 over Cu/SSZ-13 at Low Temperatures, Environ. Sci. Technol. 49 (2015) 467–473.
[17] L. Wang, W. Li, S.J. Schmieg, D. Weng, Role of Brønsted acidity in NH3 selective catalytic reduction reaction on Cu/SAPO-34 catalysts, J. Catal. 324 (2015) 98–106.
[18] L. Ma, Y. Cheng, G. Cavataio, R.W. McCabe, L. Fu, J. Li, In situ DRIFTS and temperature-programmed technology study on NH3-SCR of NOx over Cu-SSZ-13 and Cu-SAPO-34 catalysts, Appl. Catal. B Environ. 156–157 (2014) 428–437.
[19] J. Tan, Z. Liu, X. Bao, X. Liu, X. Han, C. He, R. Zhai, Crystallization and Si incorporation mechanisms of SAPO-34, Micropor. Mesopor. Mater. 53 (2002) 97–108.
[20] D. Barthomeuf, Topological model for the compared acidity of SAPOs and SiAl zeolites, Zeolites 14 (1994) 394–401.
[21] K. Leistner, L. Olsson, Deactivation of Cu/SAPO-34 during low-temperature NH3-SCR, Appl. Catal. B Environ. 165 (2015) 192–199.
[22] J. Wang, D. Fan, T. Yu, J. Wang, T. Hao, X. Hu, M. Shen, W. Li, Improvement of low-temperature hydrothermal stability of Cu/SAPO-34 catalysts by Cu2+ species, J. Catal. 322 (2015) 84–90.
[23] A. Wang, Y. Chen, E.D. Walter, N.M. Washton, D. Mei, T. Varga, Y. Wang, J. Szanyi, Y. Wang, C.H.F. Peden, F. Gao, Unraveling the mysterious failure of Cu/SAPO-34 selective catalytic reduction catalysts, Nat. Commun. 10 (2019) 1137.
[24] Y. Cao, D. Fan, P. Tian, L. Cao, T. Sun, S. Xu, M. Yang, Z. Liu, The influence of low-temperature hydration methods on the stability of Cu-SAPO-34 SCR catalyst, Chem. Eng. J. 354 (2018) 85–92.
[25] S. Huang, J. Wang, J. Wang, C. Wang, M. Shen, W. Li, The influence of crystallite size on the structural stability of Cu/SAPO-34 catalysts, Appl. Catal. B Environ. 248 (2019) 430–440.
[26] C. Niu, X. Shi, K. Liu, Y. You, S. Wang, H. He, A novel one-pot synthesized CuCe-SAPO-34 catalyst with high NH3-SCR activity and H2O resistance, Catal. Commun. 81 (2016) 20–23.
[27] X. Xiang, Y. Cao, L. Sun, P. Wu, L. Cao, S. Xu, P. Tian, Z. Liu, Improving the low-temperature hydrothermal stability of Cu-SAPO-34 by the addition of Ag for ammonia selective catalytic reduction of NO x, Appl. Catal. A Gen. 551 (2018) 79–87.
[28] Y. Cao, D. Fan, L. Sun, M. Yang, L. Cao, T. Sun, S. Xu, P. Tian, Z. Liu, The self-protection effect of reactant gas on the moisture stability of CuSAPO-34 catalyst for NH3-SCR, Chem. Eng. J. 374 (2019) 832–839.
[29] J. Woo, K. Leistner, D. Bernin, H. Ahari, M. Shost, M. Zammit, L. Olsson, Effect of various structure directing agents (SDAs) on low-temperature deactivation of Cu/SAPO-34 during NH3-SCR reaction, Catal. Sci. Technol. 8 (2018) 3090–3106.
[30] M. Briend, R. Vomscheid, M.J. Peltre, P.P. Man, D. Barthomeuf, Influence of the Choice of the Template on the Short- and Long-Term Stability of SAPO-34 Zeolite, J. Phys. Chem. 99 (1995) 8270–8276.
[31] C. Lin, Y. Cao, X. Feng, Q. Lin, H. Xu, Y. Chen, Effect of Si islands on low-temperature hydrothermal stability of Cu/SAPO-34 catalyst for NH3-SCR, J. Taiwan Inst. Chem. Eng. 81 (2017) 288–294.
[32] X. Xiang, M. Yang, B. Gao, Y. Qiao, P. Tian, S. Xu, Z. Liu, Direct Cu2+ ion-exchanged into as-synthesized SAPO-34 and its catalytic application in the selective catalytic reduction of NO with NH3, RSC Adv. 6 (2016) 12544–12552.
[33] C. Wang, M. Yang, P. Tian, S. Xu, Y. Yang, D. Wang, Y. Yuan, Z. Liu, Dual template-directed synthesis of SAPO-34 nanosheet assemblies with improved stability in the methanol to olefins reaction, J. Mater. Chem. A 3 (2015) 5608–5616.
[34] A. Izadbakhsh, F. Farhadi, F. Khorasheh, S. Sahebdelfar, M. Asadi, Y.Z. Feng, Effect of SAPO-34's composition on its physico-chemical properties and deactivation in MTO process, Appl. Catal. A Gen 364 (2009) 48–56.
[35] X. Xiang, P. Wu, Y. Cao, L. Cao, Q. Wang, S. Xu, P. Tian, Z. Liu, Investigation of low-temperature hydrothermal stability of Cu-SAPO-34 for selective catalytic reduction of NOx with NH3, Chin. J. Catal. 38 (2017) 918–927.
[36] T. Zhang, H. Chang, Y. You, C. Shi, J. Li, Excellent Activity and Selectivity of One-Pot Synthesized Cu–SSZ-13 Catalyst in the Selective Catalytic Oxidation of Ammonia to Nitrogen, Environ. Sci. Technol. 52 (2018) 4802–4808.
[37] L. Ma, Y. Cheng, G. Cavataio, R.W. McCabe, L. Fu, J. Li, Characterization of commercial Cu-SSZ-13 and Cu-SAPO-34 catalysts with hydrothermal treatment for NH3-SCR of NOx in diesel exhaust, Chem. Eng. J. 225 (2013) 323–330.
[38] L. Xie, F. Liu, X. Shi, F.-S. Xiao, H. He, Effects of post-treatment method and Na co-cation on the hydrothermal stability of Cu–SSZ-13 catalyst for the selective catalytic reduction of NOx with NH3, Appl. Catal. B Environ. 179 (2015) 206–212.
[39] Y.J. Kim, J.K. Lee, K.M. Min, S.B. Hong, I.-S. Nam, B.K. Cho, Hydrothermal stability of CuSSZ13 for reducing NOx by NH3, J. Catal. 311 (2014) 447–457.
[40] W. Su, Z. Li, Y. Peng, J. Li, Correlation of the changes in the framework and active Cu sites for typical Cu/CHA zeolites (SSZ-13 and SAPO-34) during hydrothermal aging, Phys. Chem. Chem. Phys. 17 (2015) 29142–29149.
[41] Z.W. Wu, R. Ran, Y. Ma, X.D. Wu, Z.C. Si, D. Weng, Quantitative control and identification of copper species in Cu-SAPO-34: a combined UV-vis spectroscopic and H-2-TPR analysis, Res. Chem. Intermediat. 45 (2019) 1309–1325.
[42] D. Fan, J. Wang, T. Yu, J. Wang, X. Hu, M. Shen, Catalytic deactivation mechanism research over Cu/SAPO-34 catalysts for NH3-SCR (I): The impact of 950 °c hydrothermal aging time, Chem. Eng. Sci. 176 (2018) 285–293.
[43] J. Tang, M. Xu, T. Yu, H. Ma, M. Shen, J. Wang, Catalytic deactivation mechanism research over Cu/SAPO-34 catalysts for NH3-SCR (II): The impact of copper loading, Chem. Eng. Sci. 168 (2017) 414–422.
[44] L. Wang, J.R. Gaudet, W. Li, D. Weng, Migration of Cu species in Cu/SAPO-34 during hydrothermal aging, J. Catal. 306 (2013) 68–77.
[45] S.A. Skarlis, D. Berthout, A. Nicolle, C. Dujardin, P. Granger, IR Spectroscopy Analysis and Kinetic Modeling Study for NH3 Adsorption and Desorption on H- and Fe-BEA Catalysts, J. Phys. Chem. C 117 (2013) 7154–7169.
[46] Z. Li, J. Martínez-Triguero, J. Yu, A. Corma, Conversion of methanol to olefins: Stabilization of nanosized SAPO-34 by hydrothermal treatment, J. Catal. 329 (2015) 379–388.
[47] G.A.V. Martins, G. Berlier, S. Coluccia, H.O. Pastore, G.B. Superti, G. Gatti, L. Marchese, Revisiting the Nature of the Acidity in Chabazite-Related Silicoaluminophosphates: Combined FTIR and 29Si MAS NMR Study, J. Phys. Chem. C 111 (2007) 330–339.
[48] C. Paolucci, I. Khurana, A.A. Parekh, S. Li, A.J. Shih, H. Li, J.R. Di Iorio, J.D. Albarracin-Caballero, A. Yezerets, J.T. Miller, W.N. Delgass, F.H. Ribeiro, W.F. Schneider, R. Gounder, Dynamic multinuclear sites formed by mobilized copper ions in NOx selective catalytic reduction, Science 357 (2017) 898–903.
[49] X. Hu, M. Yang, D. Fan, G. Qi, J. Wang, J. Wang, T. Yu, W. Li, M. Shen, The role of pore diffusion in determining NH3 SCR active sites over Cu/SAPO-34 catalysts, J. Catal. 341 (2016) 55–61.
[50] T. Yu, T. Hao, D. Fan, J. Wang, M. Shen, W. Li, The recent NH3-SCR mechanism research over Cu/SAPO-34 catalyst, J. Phys. Chem. C 118 (2014) 6565–6575.
[51] G. Liu, P. Tian, J. Li, D. Zhang, F. Zhou, Z. Liu, Synthesis, characterization and catalytic properties of SAPO-34 synthesized using diethylamine as a template, Micropor. Mesopor. Mater. 111 (2008) 143–149.
[52] D. Fan, P. Tian, S. Xu, D. Wang, Y. Yang, J. Li, Q. Wang, M. Yang, Z. Liu, SAPO-34 templated by dipropylamine and diisopropylamine: synthesis and catalytic performance in the methanol to olefin (MTO) reaction, New J. Chem. 40 (2016) 4236–4244.
[53] P. Tian, Y. Wei, M. Ye, Z. Liu, Methanol to Olefins (MTO): From Fundamentals to Commercialization, ACS Catal. 5 (2015) 1922–1938.
[54] Y. Qiao, P. Wu, X. Xiang, M. Yang, Q. Wang, P. Tian, Z. Liu, SAPO-34 synthesized with n-butylamine as a template and its catalytic application in the methanol amination reaction, Chin. J. Catal. 38 (2017) 574–582.